Simplified parameter extraction method for single and back-to-back Schottky diodes fabricated on Silicon-on-Insulator substrates

V. Mikhelashvili[1,2,a)], R. Padmanabhan[1,2], and G. Eisenstein[1,2]

[1]*Electrical Engineering Department, Technion, Haifa 3200003, Israel*

[2]*Russell Berrie Nanotechnology Institute, Technion, Haifa 3200003, Israel*

[a)]beso@ee.technion.ac.il

Abstract

We describe a technique to extract room temperature parameters of Schottky diodes based on single or double-terminal configurations whose barrier height is bias dependent. The method allows to extract the zero bias barrier height without specific knowledge of interface states or the existence of an insulator layers at the metal-semiconductor boundaries. The technique enables to establish the type of thermionic emission mechanism; limited by a bias dependent image force potential and / or diffusion, taking into account interfacial states or layers. The technique makes use of experimental current-voltage (I-V) characteristics measured at both bias polarities and different intensities of illumination as well as the corresponding voltage-dependent differential slope-voltage characteristics $\alpha = dln(I)/dln(V)$. The method is verified experimentally on a conventional p-Silicon based Schottky diode and on metal-semiconductor and metal-insulator-semiconductor diodes fabricated on *n*-Silicon-on-Insulator substrates. Pd/Au Schottky electrodes were used while the insulator stack of the MIS diodes comprise an HfO_2 layer on top of an SiO_2 layer.

I. Introduction

Numerous semiconductor devices and circuits make use of metal-semiconductor (MS) and metal-insulator-semiconductor (MIS) structures, or their back-to-back (MSM or MISM) configurations [1]. MS junctions exhibit either an Ohmic or a rectifying behavior; this is determined by the work-function of the metal (ψ_m), the electron affinity of the semiconductor (χ_S), the interfacial-trap density at the MS junction, the thickness of an interfacial layer (when such layer exists) and the potential barrier. All these factors influence the barrier height, which ideally is the difference between metal work function and electron affinity of the *n*-type semiconductor [2]: $\varphi_{bn} = \psi_m - \chi_S$, while for p-type semiconductor the $\varphi_{bp} = E_g - (\psi_m - \chi_S)$, where E_g is the band gap of the semiconductor. The Ohmic or rectifying nature of a junction can be altered by a bias voltage as well as illumination, temperature, and radiation. These external perturbations manifest themselves as a modification of the current-voltage (I-V) characteristics of the device. In the case where both electrodes form Schottky-type contacts in a MSM system, the carrier transport mechanism is complex; in particular, if the junctions are asymmetric (due to the use of electrode materials with different ψ_m, and or due to the presence of an intefacial insulator layer between the electrode and semiconductor [3]). Double-Schottky MSM diodes and heterojunctions with different barrier heights were analysed in [4, 5] by employing the thermionic emission theory model, which is valid for semiconductor substrates with doping levels, $N_{A,D,}$ below 10^{17} cm^{-3} [6-8].

The influence of illumination on φ_{bn}, and therefore, on the photosensitivity of photodetectors was considered in Refs. 9-13. The reduction of φ_{bn} under illumination, in conjunction with the lowering of the potential barrier due to image-forces, was attributed to the change in the quasi-Fermi level in the semiconductor relative to the dark equilibrium state [10]. This was also used to explain the observed photosensitivity of I-V and capacitance-voltage (C-V) characteristics in MIS diodes [2, 14)]. Variations in different Schottky-barrier parameters also influence the photosensitivity of different MSM and MIS structures [11-13]. MIS structures with a leaky insulator stack containing many pores (metal seeping through the pores result in the formation of local MS junctions) was considered in [11]. Under illumination, photo generated holes are accumulated at the Si surface along the perimeter of the islands, enhancing the electric field around specific local points thereby lowering φ_{bn}, which increases in turn the photosensitivity.

The photocurrent intensification in MIS structures can also be attributed to edge fringing field effects [12,13].

Most of the earlier published papers [15-21] use graphical methods to extract parameters from forward biased I-V characteristics of Schottky diodes. All the extracted parameters: ideality factor, saturation current, zero-bias barrier height (when the value of linear series resistance is known), assumed to be independent of the applied voltage. In [22], these parameters were extracted using the voltage difference of differential slope (α–V, where $\alpha = {d(lnI)}/{d(lnV_R)}$) of

I-V characteristics, additionally taking into consideration the non-linear series resistance and parallel conductance. A complex graphical differentiation of the experimental forward bias I-V characteristics was employed in [23, 24], in order to extract voltage-dependent ideality factor, after the extraction of surface states and traps in the interfacial layer between the Schottky electrode and semiconductor. Finally, [25] analyzed the α–V characteristics, which enabled the extraction of the linear series resistance and voltage-dependent ideality factor from the experimental I-V characteristics. However, this method assumes that the change of the image potential with applied voltage is linear, which is valid only at small biases [26].

The strong influence of the barrier height on the characteristics of the devices comprising Schottky electrodes call for a more effective method, than those discussed above, to evaluate the role of the electrode materials and geometry as well as the effect of external perturbations. To this end, we have developed a comprehensive procedure, which in contrast with earlier studies allows establishing, from the reverse bias I-V characteristics, the most probable current flow mechanisms in a Schottky junction; thermionic emission limited or diffusion limited in the presence or absence of surface states at the metal-semiconductor boundary or without them in conjunction of an image force. Also determined are the image force potential and the zero voltage barrier height of holes (φ_{bp0}) or electrons (φ_{bn0}), as well as their modification with illumination. The method was verified for MS, MSM and MISM structures with symmetric or asymmetric electrodes by measurement of the current voltage characteristics (I-V) at room temperature under different illumination regimes. The developed method requires the knowledge of doping level of substrate only, with the assumption of mono energetic or uniformly distributed

in energy within the bandgap of surface states [1, 26-28] with a constant density. For other types of distribution of interface states, it is essential to identify the distribution behavior [29, 30].

II. Theoretical analysis

The planar systems analyzed in this paper include pairs of diodes connected back-to-back via the silicon. Sytems comprising of p-Si can be analyzed similarly. A simplified equivalent circuit of such a structure is shown in Fig.1, where V_1 and V_2 are the voltage drops across diodes I and II, respectively. This model is based on the assumption that the voltage drop across the Si can be neglected, when compared to the voltage drop across the reverse-biased diode junction namely, the applied voltage equals $V = V_1 + V_2$. Based on current continuity theory, the total current density $J_T = J_1 = J_2$ (for the system represented in Fig.1) is given by [4, 5]

$$J_T = \frac{2J_{s1}J_{s2}\sinh(^{qV}/_{2kT})}{J_{s1}\exp\left(^{qV}/_{2kT}\right)+J_{s2}\exp\left(-^{qV}/_{2kT}\right)} \quad (1)$$

where, J_{s1} and $J_{s2}$are the leakage current densities through the reverse-biased Schottky junctions I and II, respectively; while *T*, *q*, and *k* are the absolute temperature, electron charge, and Boltzmann constant, respectively, while current density: $J = {}^{I}/_{S}$, where *S* is electrode area.

One of the diodes *I* or *II* is always reverse biased and hence limits the net current for either bias polarity. J_{s1} and J_{s2} at a reverse-biased Schottky junctions with unequal barrier heights are [1, 27, 28]

$$J_{s1}, J_{s2} = \frac{\theta q N_{v,c}\, \upsilon_R \exp\left(-^{q\varphi_{bp1,n1},q\varphi_{bp2,n2}}/_{kT}\right)}{\left(1-\frac{\theta \upsilon_R}{\upsilon_D}\right)} \quad (2)$$

where $\varphi_{bp1,n1}$ and $\varphi_{bp2,n2}$ are the voltage-dependent barrier heights at the junctions *I* and *II*, respectively, υ_R and υ_D are the thermal and effective diffusion velocities of carriers, respectively, N_v and N_c are the effective density of states in the valence or conduction bands, respectively and θ is the barrier transmission coefficient ($\theta < 1$ or $\theta = 1$, for barriers with or without an

interfacial layer, respectively). The relation of thermal and effective carrier diffusion velocities determines the role of the thermionic emission or diffusion current flow mechanisms.

Leakage current density in an ideal Schottky diode is independent of the applied reverse-bias; it is determined only by $\varphi_{bp,n} = \varphi_{bp0,n0}$. However, real Schottky diodes exhibit a significant increase in leakage current with reverse bias due to the voltage-dependence of the Schottky barrier height. The increase in leakage current is larger than that caused by thermally-generated minority carriers within the expanding depletion region. The Schottky barrier height is reduced in the dark due to both a variation of image force potential and a dipole layer, which results from an interfacial layer with surface trap states and or fixed charges at the MS boundary [1, 27, 28]. The barrier height reduces further under illumination [10]

The variation of the $q\varphi_{bn}$ is generally expressed as [9, 27, 28]

$$\varphi_{bp1,n1,}\varphi_{bp2,n2} = \varphi_{bp01,n01}, \varphi_{bp02,n02} \pm \Delta\varphi, \quad (3)$$

Where

$$\Delta\varphi = \left(1 - \frac{1}{n_0}\right) V_R + \Delta\varphi_0 + \Delta\varphi^{ill} \quad (4)$$

The interfacial layer, image force and illumination related contributions are

$$\frac{1}{n_0} = \frac{\varepsilon_0 \varepsilon_i}{\varepsilon_0 \varepsilon_i + q^2 d_i D_{it}}, \quad (5)$$

$$\Delta\varphi_0 = \left(\frac{q^3 N_{A,D}}{8\pi^2 \varepsilon_0^3 \varepsilon_S^3}\right)^{1/4} \left[\left(V_{bi} + |V_R| - \frac{kT}{q}\right)^{1/4}\right] \quad (6)$$

and

$$\Delta\varphi^{ill} = (E_{fn}^{ill} - E_f) \text{ or } \Delta\varphi^{ill} = (E_f - E_{fp}^{ill}) \quad (7),$$

respectively, for n and p type semiconductors.

The ± sign in (3) denotes forward (V_F) and reverse (V_R) bias, respectively. $\varepsilon_0, \varepsilon_i$ and d_i are the free space permittivity, dielectric constant and thickness of the interfacial layer while D_{it} is the density of the surface states per unit energy and area. Surface states are assumed to be uniformly

distributed in energy within the bandgap. $V_{bi} = \psi_s - \psi_m + \frac{kT}{q}\ln(\frac{N_v}{N_A})$ and $V_{bi} = \psi_m - \psi_s - \frac{kT}{q}\ln(\frac{N_c}{N_D})$ and N_A, N_D, are the built-in voltages (or diffusion potentials) and the acceptor donor concentration, respectively of p or n type semiconductors; ψ_s is the work function of the semiconductor. $\varphi_{bn01,}\varphi_{bn02}=(\psi_{m1}, \psi_{m2} - \chi_s)$ are the barrier heights at zero bias; ψ_{m1} and ψ_{m2} are the work functions of the metal electrodes. The corresponding hole barrier heights are $\varphi_{bp01,}\varphi_{bp02}=\frac{1}{2}E_g - (\psi_{m1}, \psi_{m2} - \chi_s)$, where E_g is the semiconductor band gap. E_F, E_{fn}^{ill} and E_{fp}^{ill} are the equilibrium Fermi and quasi Fermi levels of electrons or holes under illumination while $(E_{fn}^{ill} - E_f) = kTLn(n_i^{ill}/N_D)$, $(E_f - E_{fp}^{ill}) = kTLn(n_i^{ill}/N_A)$ with n_i^{ill} the illumination intensity dependent intrinsic carrier concentration [10].

At small D_{it}values, when $\varepsilon_o\varepsilon_i \ll q^2 d_i D_{it}$ (see Eq. 5), the barrier height changes by the image force. The relation of thermal to diffusion velocities distinguishes between two limiting Schottky current mechanisms in MSM or MIS structures. When $\theta v_R \ll v_D$ (see Eq.2), only thermionic emission determines the current flow while for large θv_R values, carrier diffusion from the edge of the depletion layer to the peak of the image force potential (electrostatic potential of the conduction band) limits the current. Inserting equations (3) and (4) into (2) leads to several current transport mechanisms that take place in real Schottky diodes and therefore in pairs of back-to-back connected devices. The thermionic and diffusion mechanisms in reverse biased Schottky diodes (taking into account an interfacial layer and the transmission coefficient of the barrier to be smaller than unity [27, 28]) are approximated by:

$$J_{s,thermionic} = \theta A^* T^2 \exp\left(-\frac{q\varphi_{bp0,n0}}{kT}\right)\exp(\frac{q\Delta\varphi}{kT}) \qquad (8)$$

$$J_{s,diffusion} = q\mu N_{v,c}(\frac{2qN_{A,D}}{\varepsilon_0\varepsilon_s})^{1/2}(V_{bi} - V_R)^{1/2}\exp\left(-\frac{q\varphi_{bp0,n0}}{kT}\right)\exp(\frac{q\Delta\varphi}{kT}) \quad (9)$$

Where A^* is the effective Richardson constant (for *n-Si*, A^*=120m^*_e; m^*_e being the effective mass of the electron). Based on equations (3) to (6), we propose a simple analytical method to analyze experimental current-voltage characteristics in order to discriminate among the carrier

transport mechanisms (thermionic or diffusion with or without the influence of an interfacial layer) and to extract the zero bias Schottky barrier height and the voltage dependence of the image force.

We analyze the $\boldsymbol{\alpha}$-V curves, whose usefulness in the extraction of the diode parameters was demonstrated in [22, 25, 31-36]. The technique we propose does not require to resort to complicated graphical differentiation techniques as given in [23, 24]; and it is unlike the technique shown in [37], which are only valid under limited conditions.

Simple algebraic manipulation of equations (8) and (9) yields two pairs (for the thermionic and diffusion cases) of analytical expressions of α-V_R in order to extract the values of voltage dependent lowering of the barrier height (with or without interfacial states influence**).** These equations are summarized in Table 1.

Table 1. Extraction of the exponential coefficient (equations (8) and (9)) bias dependent $\Delta\varphi$ at different current flow mechanisms of the thermionic emission.

Conditions	Current flow mechanisms	$\alpha - V_R$ dependence	$\Delta\varphi, eV$
Without interfacial layer or states	Thermionic limited current, taking into account image force potential ($\theta v_R \ll v_D$)	$\alpha = \frac{qV_R}{kT}\frac{d(\Delta\varphi)}{dV_R}$	$\frac{kT}{q}\int_{V_R=0}^{V_R}\frac{\alpha}{V_R}dV_R + C_1$ $\Delta\varphi = \Delta\varphi_0$ (10)
Without interfacial layer or states	Diffusion limited thermionic current ($\theta v_R \gg v_D$)	$\alpha = \frac{qV_R}{kT}\frac{d(\Delta\varphi_0)}{dV_R} - \frac{1}{2}\frac{V_R}{(V_{bi}-V_R)}$	$\frac{kT}{q}\{\int_{V_R=0}^{V_R}\frac{\alpha}{V_R}dV_R - \frac{1}{2}\ln(\lvert V_{bi}-V_R\rvert)\} + C_1 + C_2$ $\Delta\varphi = \Delta\varphi_0$ (11)

With interfacial layer or states	Thermionic limited current ($\theta v_R \ll v_D$)	$\alpha = \frac{qV_R}{kT}\frac{d(\Delta\varphi)}{dV_R}$	$\frac{kT}{q}\int_{V_R=0}^{V_R}\frac{\alpha}{V_R}dV_R + C_1$ $\Delta\varphi = \left(1-\frac{1}{n_0}\right)V_R + \Delta\varphi_0$ (12)

The behavior of the calculated reverse *I*-V_R and α–V_R characteristics in all the particular cases considered above are summered in Fig.2. As predicted by equation (1), the total current in back-to-back connected diodes is limited by the reverse biased diode, while the influence of the forward direction biased diode is insignificant due to its low differential resistance.

The *I*-V_R characteristics of structures with equal ($\varphi_{bn01} = \varphi_{bn02} = 0.8\,eV$) and unequal ($\varphi_{bn01} = 0.8\,eV\ and\ \varphi_{bn02} = 0.73\,eV$) barrier heights, reveal symmetric and asymmetric characteristics (see curves 1 and 2) in Fig. 2(a), respectively. Curve 1 and 2 were calculated considering the thermionic emission limited case and lowering of the barriers height only by the voltage dependent image force. The consequent α–V_R characteristics (Fig. 2(b)) is symmetric in both cases independent of the barrier heights difference. The reason is that the differential slope value and its change with applied reverse voltage are determined only by the variation of the image force potential. When the diffusion limited current dominates, for equal zero biased barrier heights, the total current is more than one order of magnitude larger than in the thermionic emission case. The dependence of the pre-exponential term on applied reverse voltage (see equation (9)) causes the differential slope to change fast with applied bias as compared with the thermionic emission case. The transition regions in both current flow mechanisms are almost linear (α values at zero bias approaches 1). The *I*-V_R curves were calculated next for diodes, which includes a thin interfacial layers at the metal semiconductor interfaces. The calculation assumed again equal barrier heights. The voltage dependence of the reverse current on applied voltage is symmetric once more but with larger values that increase exponentially with bias. This is also exhibited in the α–V_R behavior (see curve 4 in Fig. 2b),

which is linear with applied voltage, in contrast to cases without an interfacial layer, and also depends strongly on the density of the interface states.

Solving numerically two equation system that include eq. (4) and the expression of the differential slope

$$\alpha = \frac{|V_R|}{kT}\left[\left(1-\frac{1}{n_o}\right)-\frac{d\Delta\varphi_o}{dV_R}\right], \text{(13a)}$$

$$\frac{d\Delta\varphi_o}{dV_R} = \frac{1}{4}\left(\frac{q^3 N_{A,D}}{8\pi^2\varepsilon_o^3\varepsilon_s^3}\right)^{1/4}\frac{1}{\left(V_{bi}+|V_R|-\frac{kT}{q}\right)^{3/4}} \text{(13b)}$$

enables to estimate the values of $\left(1-\frac{1}{n_o}\right)$ from experimental data and hence D_{it} used in equation (5). Equation (13a) is obtained from eq. (8), taking into account that $\Delta\varphi$ in (4) is affected by interfacial states and the image force potential as in equations (5) and (6).

The value of $\Delta\varphi$ extracted from experimental *I*-V_R and α–V_R characteristics in accordance with the proper equations of the table enables calculation of the zero biased barrier height from equations (8) or (9)

$$\varphi_{bp0,n0} = kTln\left(\frac{I}{AS}\right) - \Delta\varphi \text{ (14)},$$

where *I* and *A* are the measured total current and the pre-exponential multiplier in (8) and (9), respectively. There are several difficulties in establishing accurately the contact parameters in the case where a thin insulator layer exists between the metal and the semiconductor. The difficulties stem from the fact that the measured leakage current is sensitive to local non-uniformities (non-uniform thickness, crystalline inclusions embedded into the amorphous matrix or grain boundaries). In addition, when the films are subjected to a high electric field, injection into insulator may modify the insulating properties permanently even in the absence of local non-uniformities. This makes it impossible to determine the actual electrode area contacting non-uniform current channels, which actually defines the measured current density and therefore the Schottky barrier height in accordance with equation (14). The transmission coefficient, which is usually assumed to be about 1, may reduce from this ideal value under large electric fields (>> 1 MV/cm) due to auto electron emission phenomenon [8, 38]. However, even an error in determination of the area or θ by factor of 10 can vary the actual barrier height by only ~12 %

due to the logarithmic term in equation (14). Note, that the image force potential value is not function of the real area of the electrodes and transmission coefficient. Thus, the method allows to establish the value and the trend of the barrier height dependence on illumination with satisfactory accuracy.

III. Experimental verification

The parameter extraction technique and discrimination among transport mechanisms were employed in three different Schottky devices. A commercial n-Si Schottky diode (MA40147-213) and two experimental planar structures fabricated on Silicon-on-Insulator (SOI) substrates; one being a symmetric back-to-back connected metal-semiconductor-metal (MSM) structure and the second a metal-insulator-semiconductor-metal (MIS-MS) diode which is asymmetric.

The SOI substrate included a 3 μm thick n-Si device layer with a resistivity of 50 **Ω**cm and a 1.4 μm thick SiO_2 box layer. The MSM and MIS-MS structures comprised similar electrodes; an electron beam gun evaporated Pd/Au stack, which ensured a high potential barrier. The insulator stack included a 3 nm thermal SiO_2 covered by an Atomic Layer deposited 20 nm HfO_2 film. Pt nanoparticles growth in-situ with the HfO_2 film were embedded between the two insulator layers. The measurement of the SOI based devices were carried out in the dark and under illumination at 365 nm. The optical signal was applied via a fiber lens. The electrodes area in the MSM diode was $1.6x10^{-5}$ cm^2 with an inter electrodes distance of 20 μm which was illuminated uniformly with a spot area of $1.7x10^{-6}$ cm^2. In the MIS-MS structure, only the MIS branch was illuminated. In order to ensure the asymmetric illumination, the inter electrode distance was increased to 135 μm where the electrodes were connected via the silicon device layer. The electrode area in the MIS diode was $1.75x10^{-6}$ cm^2. A schematic image of the measured structure is similar to that described in [3].

The MIS-MS structure underwent a voltage stress process [14] in order to form filament paths, which enable a leakage path for the photocurrent. All the experiments were conducted for a variable gate voltage and a grounded back electrode. The I-V characteristics were measured at room temperature using an Agilent 4155C Semiconductor parameter analyzer.

1. Single Schottky diode

Measured I-V characteristics of a commercial Schottky diode and the corresponding calculated α-V characteristics are shown by solid lines in Fig. 3a, b. The typical exponential behavior at forward bias and saturation under reverse bias conditions are clearly observed. The more sensitive α-V dependences reveal a very small α value of 0.08-0.11 (see insert in Fig. 3 (b)) under reverse bias while in the forward bias case, α is larger than 1 over a limited voltage range and eventually reaches a peak when the current is limited by the MS junction barriers. At this point, the current flow mechanism changes from exponential to one that is dominated by the series resistance of the bulk semiconductor and the Ohmic back contact.

The parameters of the maximum point *(α_{max}, V_{max} and I_{max})* enable extraction of the ideality factor, total barrier height φ_{bn} and series resistance [22] which in the present case are 1.12, 0.65 eV and 0.89 **Ω**, respectively. An ideality factor value of about 1.12 was estimated from the maximum of $\boldsymbol{\alpha}$-V plot in accordance with method described in Ref.22, which assumes the Schottky barrier height to be independent of the applied voltage. Therefore, the extracted ideality factor value is an approximate one. The real voltage dependence of the ideality factor, in accordance with [1, 26], is expressed as: $n \approx 1/(1 - {}^{d\Delta\varphi}/_{dV})$, assuming voltage independent Richardson coefficient. A correct curve depicting the dependence of the ideality factor with applied bias is shown in the Fig. 3(d), which takes the voltage-dependence of the extracted image force potential into account (see Fig. 3(c)). It is seen that *n* reduces from 1.027 at $V > 0.05\,V$ to 1.005 at $V = 0.4\,V$. Therefore, the small deviation of the ideality factor from 1 can certainly be attributed to the influence of image force potential. A similar procedure can be used to establish the behavior of the ideality factor with applied bias in the common case (see Eq. (4)) when interfacial states are present with or without incorporation of the image force potential.

The small deviation of the ideality factor from a value of unity indicates that the current flow by thermionic emission is disturbed by the effect of the voltage dependent image force potential [1, 26]. This is further proven by the weak dependence of α on the reverse bias. Moreover, $\alpha \ll 0.5$

(at reverse bias) indicates that diffusion limited thermionic emission (which is characterized by $\alpha \approx 0.5$) does not take place. In addition, interfacial states (or a thin interfacial insulator layer) at the metal-semiconductor interface are also absent since α does not depend linearly on the applied voltage. Further evidence lies in the linear dependence on $V_R^{1/4}$ of the $\Delta\varphi$ value, extracted by the equation (10) appearing in table 1 and shown in Fig. 3 (c). This indicates that the thermionic emission mechanism with voltage modified image force potential dominates (see eq. (6)). The zero bias barrier height, estimated by equation (14), taking into consideration equation (4), is $0.64\ eV$. It differs from the value obtained from the forward bias I-V characteristics which is the sum of the $\varphi_{bno} + \Delta\varphi_o$ (see eq. (3)) and takes on the value of 0.65 eV. The calculated I-V and α–V curves (which use the extracted parameters, when θ = 1) are plotted in Fig. 3 (a) and 3 (b) as dash lines. The inset shows the reverse bias portion of the α–V plot, in a magnified scale. The perfect coincidence testifies to the strength of the proposed method, which is simpler than the complicated current versus temperature technique of extraction, zero bias barrier height of single Schottky diodes [1].

2. Back-to-back connected structure with symmetric Schottky electrodes

Next, we examine the proposed technique for MSM diodes operating in the dark and under illumination. Experimental I-V and α–V curves are shown in Fig. 4 (a) and (b).

As predicted by equations (1) and (2) (see Fig. 2 (b)), the I-V characteristics are saturated for both bias polarities for $|V| > 0.8\,V$. For bias levels smaller than 0.8 V and independent of illumination, α increases as the bias is reduced and at |V|=0 V it reaches unity.

A qualitative analysis of the experimental α–V characteristics indicates that it is consistent with the theoretical curves shown in Fig. 2 (b) (α measured in the dark is approximately 0.45). At large voltages, α saturates with the average value reducing from 0.45 in the dark to 0.2 within a small range of illumination intensities of less than $4\text{x}10^{-8}$ Watt. In the illumination range of $4\text{x}10^{-8}$ Watt to $2.5\text{x}10^{-6}$ Watt, α varies in the small range of 0.1-0.2. We conclude that under low illumination, the current flow mechanism is close to diffusion-limited thermionic emission

(where α~0.45 which is close to the theoretical of 0.5) with the incorporation of bias dependent image force potential. However, increasing the illumination intensity leads to thermionic emission, which is limited only by barrier height variation due to image force potential changes with applied voltage. The measured sub-linear character of $\alpha - V$ for all bias levels precludes any role of interfacial states or an interfacial layer at the metal-semiconductor interfaces similar to that observed for the single Schottky diode discussed above. The reason is that interfacial states would lead to an exponential dependence of the reverse saturation current on applied voltage and therefore a linear increase of α with applied voltage, as predicted by equations (2) or (8) taking into consideration (3) and (4).

Fig. 4 (c) and (d) present extracted $\Delta\varphi$ and experimental $Ln(I)$ versus $V_R^{1/4}$ in the dark and illumination regimes. The linear character of the curves indicates that only variations of the image force potential with applied bias limits the voltage dependence of the exponential part of the I-V characteristic, in accordance with equations (6) and (8).

$\Delta\varphi = \Delta\varphi_o$ calculated from the experimental *I-V* and α–*V* curves, using the equations of table 1, increases with illumination (see Fig 4 (c)) but maintains the linear $V_R^{1/4}$ dependence similar to the dark regime. In the dark and at small illumination powers, $\Delta\varphi_o$ values were extracted by the equation (11) in table 1 while at large illuminations, we used the equation (10). This causes a reduction of the zero biased dark barrier height in both bias polarities from 0.68 eV to 0.525 eV. The illumination power dependences of the zero bias barrier heights, calculated for both bias polarities with and without diffusion, limited thermionic emission regimes are shown in Fig. 4 (e). As expected, the dependencies are similar due to the identical metallic stack used in both electrodes. The small difference in the extracted curves are due to deviations from uniform illumination of the inter electrodes area.

The enhancement of thermionic emission of carriers into the semiconductor under illumination due to lowering of the barrier height was discussed in [9, 39, 40]. Illumination induces a difference between the quasi-Fermi level of the photo-excited holes in the depletion region of an n-type semiconductor and the equilibrium Fermi level. Under illumination, the full reduction of the barrier height should be considered in eq. (4) and (7).

Fig. 5(a) and (b) compares the experimental (symbols) and calculated (dash lines) I-V and α–V curves, in the dark and under maximum illumination. The curves were calculated according to equations (9) and (14) using the extracted parameters from the experimental I-V characteristics. The agreement of calculated and experimental curves, especially in the saturation regime, as well as their similar behavior to the simulated results of Fig.2 is quite remarkable. Finally, we note that the measured symmetrical I-V and α-V characteristics with zero photo current at zero bias is due to the zero electric field at the center of the potential well caused by the two identical rectifying electrodes. This is in contrast to the single Schottky photo diode where at zero bias, the internal electric field formed by the work function difference between metal-semiconductor induces a finite photocurrent [1].

3. Back-to-back connected MIS and MS structures with asymmetric junctions and illumination

I-V characteristics of a MIS-MS structure measured are shown in Fig. 6 (a). The illumination was non-uniform: the MIS part of device was illuminated while the MS section is in the dark.

The first difference from the MSM data (see Fig. 4 (a) and (b)) is (see Fig. 6 (a) and (b)) that at negative bias, conventional photocurrent with illumination is observed while at positive bias, it is significantly lower although it is higher than the dark current. The effect of illumination on the MS junction current (which is in the dark) is due to drift-diffusion via the Si layer of the photo generated minority carriers from the positive biased illuminated gate area, while MS junction is under negative polarity of the voltage [41]. Minority carriers that accumulate at the MS interface attract majority carriers from the reverse biased electrode and hence causes an increase in the net current [2].

The second difference is that under illumination and negative bias, the I-V curve changes super linearly. This is clearly seen in Fig. 6 (b) (see inset with curves enlarged along the voltage scale), where the $\boldsymbol{\alpha}$-V curves, measured in the dark and under illumination, reaches large values in the vicinity of zero bias. For positive bias, the behavior is similar to that of the MSM structure

(see Fig. 4 (b)). The $\boldsymbol{\alpha}$-V curves under illumination are linear and in the bias range of 0 V to -0.65 V (see linear fit in the inset of Fig. 6 (b)), while for -1.5 V to -5 V they are sublinear. For both bias polarities in the dark regime, and for positive bias under illumination, a region with $\alpha \ll 0.5$ is observed similar to the MSM structure (see Fig. 4 (b)).

We postulate that the reason for the change in the nature of the contact from rectifying (where $\alpha \ll 1$) under reverse bias and in the dark to injecting (with $\alpha > 1$) under illumination is an accumulation of photo generated minority carriers at the semiconductor surface, which attract majority carriers from the gate electrodes so as to ensure charge neutrality across the junction. The almost linear character of α-V (see inset in Fig. 6 (b)) is due to the contribution of interfacial traps in the thermionic emission process, in accordance with eq. (4). This however cannot explain the revelation of a maximum point in the $\boldsymbol{\alpha}$-V curves. The super linearity of the I-V characteristics can also be induced by the space charge limited current due to filling of interfacial or bulk traps originating from the filamentation process and the Pt NPs. In the low voltage range, the gate electrode has a limited capacity to supply external carriers; the drop of the $\boldsymbol{\alpha}$-V curve following the maximum can only be induced by such a change in the capability of the electrode to supply excess carriers. In accordance with [7, 42, 43], when the current is sufficiently high, or when the electric field at the metal-semiconductor interface gap is large, the real value of the effective contact concentration formed close to the semiconductor surface decreases and therefore the character of the current flow mechanism change from limited by traps to Schottky barrier height. All these effects result in a non-monotonic $\boldsymbol{\alpha}$-V curve seen in Fig. 6**.** Enhancement due to illumination of the local electric fields in MIS structures with ultra-thin porous insulators compared to uniform films was discussed in [11], while a similar effect due to edge fringing fields in the vicinity of the electrodes were considered in [11-13]. A comparable increase of the local electric field in the filament regions of the insulator stack is expected at negative voltages (|V|>1.5 V), corresponding to the saturation region of the I-V characteristics ($\boldsymbol{\alpha}<1$).

It is seen in Fig. 6 (b) that in the dark regime, reduction and saturation of α in both bias polarities, is observed imediatly after the maximum at $\alpha \cong 1$ (analogoue to curves in Fig. 2 (b) or Fig. 5 (b)) in a very small voltage range close to zero. The explanation is that the bulk carrier concentration in the Si layer is not pertrubated by the externally injected carriers, whose density

is limited by the large barrier height and are exclusively captered by interfacial traps. The reason for the weak voltage dependence of the current and therefore the small values of α in both bias polarities is analogues to the MSM case where the image force potential affects the barrier height.

At negative bias on the MS part of the device, the influence of illumination and interfacial layer are negligible and hence α–V behaves analogous to the MSM structure or the dark regime. The maximum $\boldsymbol{\alpha}$-V value at very small bias (see inset in Fig. 6 (b)) is not due to the interfacial states at the MS boundary but rather due to a change in the sign of the current at the inflection point close to zero bias. Finally, the diffusion mechanism is excluded as the $\boldsymbol{\alpha}$ at any applied bias differ significantly from the theoretical value of 0.5.

Fig. 7 describes the influence of illumination power on the lowering of the barrier height in both junctions: MIS and MS. At any illumination power, the determination of the zero bias barrier height at negative bias assumes that two factors determine the exponential factor: the presence of interfacial states and an image force potential. Therefore, using experimental I-V and $\boldsymbol{\alpha}$-V curves and the procedure given in equation (12) of table 1, we extract $\Delta\varphi$ (see equation (4)) and hence the barrier height. At positive bias, the voltage dependence of the barrier height is only limited by the image force potential (see equation (10) in table 1). Fig. 7 clearly demonstrates the effect of the non-uniform illumination on the asymmetric variation of the barrier heights in the gate and back electrodes, as the net current is different in different branches (MIS and MS). In dark, the zero bias barrier heights are almost identical: of about 0.7 eV and 0.71 eV. However, a significant deviation in zero bias barrier height is already clearly observed at small illumination powers of about 1.0×10^{-9} W.

IV. Conclusions

We presented a new method for the extraction of the zero bias barrier height and for the reproduction of the image force potential dependence on voltage of a single and back-to-back connected Schottky structures, from experimental I-V characteristics. Translation of the I-V characteristics to the voltage dependent differential slope curve establishes the dominant thermionic emission mechanisms among alternative ones (limited by diffusion, bias varied image

force potential, interfacial states or their combinations). We show successful fitting of the current–voltage dependences of different structures by parameters extracted from experimental I-V curves measured at different illumination regimes. The advantage of the proposed technique over other published methods [1, 5, 40] is that the zero bias barrier height of Schottky diodes used in single or back-to-back configurations without assuming that interfacial states or insulator layer exist, even at room temperature. Together with the method developed earlier in [22, 25], it is possible using the forward I-V characteristics additionally to determine the ideality factor and the series resistance of a single Schottky diode.

Figure captions

Fig. 1 The schematic electrical circuit of a back-to-back connected pair of diodes (R_{Si} is the *Si* layer resistance).

Fig. 2 (a) Current-voltage and (b) α-V characteristics of the back-to-back connected MS diodes simulated in accordance with equation (1) for different current flow mechanisms descripted by equations (8) and (9). Curves 1 and 2-thermionic emission limited current, respectively for equal $\varphi_{bn01} = \varphi_{bn02} = 0.8\,eV$ and different $\varphi_{bn01} = 0.73\,eV$ and $\varphi_{bn02} = 0.8\,eV$, zero biased barrier heights; curves 3 and 4, respectively in the cases of diffusion limited current and thermionic limited current at availability of the interfacial layer or states, while with equal barrier heights ($\varphi_{bn01} = \varphi_{bn02} = 0.8\,eV$). The rest calculation parameters are: A^*=120m_e^* $Acm^{-2}K^{-2}$, T=300 K, N_D=8x10^{13} cm^{-3}, N_c=2.8x10^{19} cm^{-3}, θ=1, V_{bi}=0.82 eV, ε_s= 11.8, μ=1400 $cm^2V^{-1}s^{-1}$, D_{it}=1x10^{11} $cm^{-2}eV^{-1}$, d_i=3 nm and S=3.4e-6 cm^2.

Fig. 3 Experimental (symbols) and calculated (dash lines) (a) current-voltage and (b) α-V characteristics of a single Schottky diode measured in dark. The inset shows the α-V dependence in an enlarged scale; (c) Extracted image force potential versus $V_R^{1/4}$ (symbols) and linear fit curves (dash line); (d) Extracted ideality factor versus applied voltage.

Fig. 4 A set of experimental (a) current-voltage and (b) differential slope-voltage characteristics of a planar MSM structure with symmetric metallic electrodes, measured in the dark and under illumination; (c) Image force potential extracted from experimental data; (d) logarithm of the experimental current dependences on $V_R^{1/4}$ and the linear fit in the dark and under illumination

power of $2.5x10^{-6}$ Watt; (e) Zero bias barrier height versus illumination power extracted from I-V and $\alpha-V$ at both bias polarities.

Fig. 5 Experimental (symbols) and calculated (solid lines) (a) current-voltage and (b) differential slope-voltage characteristics of the MSM structures measured in the dark and under illumination at $2.5x10^{-6}$ Watt. Calculation in the dark regime and under illumination considered the extracted image force potential assuming thermionic emission with and without limitations by diffusion and the absence of interfacial states or layers. In the calculation, the extracted values of φ_{bn0} equal to: 0.69 eV in dark and 0.525 eV under illumination were used. The other parameters of calculation in equations (2), 8 and (9) are: $\theta = 1$, A^*=120m^* $Acm^{-2}K^{-2}$ and T=300 K.

Fig. 6 The experimental (a) current-voltage and (b) differential slope-voltage characteristics of a planar MISM structure on SOI substrate with identical metallic electrodes, measured in the dark regime and under illumination. The inset shows the part of the α-V curves measured at small voltages, while the dash line is a linear fit.

Fig. 7 The dependence of the zero bias barrier height on illumination power in the case of an asymmetric illumination of the branches of the MISM structure.

References

[1]S.M.Sze and Kwok K. Ng, Physics of Semiconductor Devices, 2006, John Wiley & Sons, New York.

[2] N.F. Mott, Proc. Camb. Philos. Soc. 34, 568 (1938).

[3]V Mikhelashvili, R Padmanabhan, B Meyler, S Yofis, G Eisenstein, J. Appl. Phys. 120, 224502 (2016).

[4]X.-L. Tang, H.-W. Zhang, H. Su, Z.-Y. Zhong, Physica E, 31,103 (2006).

[5] A.J. Chiquito, C.A. Amorim, O.M. Berengue, L.S. Araujo, E.P.Bernardo, and E.R.Leite, J.Phys.: Condens. Matter., 24, 225303, (2012).

[6]C.R. Crowell and S. Sze, Solid State Electronics, 8, 1035 (1966).

[7] F.A. Padovani, Solid State Electronics, 12, 135 (1969).

[8] A.N. Zyuganov and S.V. Svechnikov, Injection contact phenomena in semiconductors, Naukova Dumka, Kiev, 1981, [in Russian].

[9]T.Y. Chen and J.G. Hwu, ECS Journal of Solid State Science and Technology, 3, Q37 (2014).

[10]Q.Yang, X.Guo, W. Wang, Y. Zhang, S.Xu, D.H. Lien and Z.L. Wang, ASC Nano, 4, 6285 (2010).

[11]O. Malik, V. Grimalsky and J. De La Hidalga-W, Sensors and Actuators A: Physical, 130, 208 (2006).

[12]C.Y. Yang and J.G. Hwu, IEEE Sensors Journal, 12, 2313, (2012).

[13]T.Y. Chen and J.G. Hwu, Appl. Phys. Lett., 101, 073506 (2012).

[14]V. Mikhelashvili, D. Cristea, B. Meyler, S. Yofis, Y. Shneider, G. Atiya, J. Appl. Phys., 116, 074513 (2014).

[15]H. Norde, J. Appl. Phys. 50, 5052 (1979).

[16]C. D. Lien, F. C. T. So, and M. A. Nicolet, IEEE Trans. Electron Devices ED-31, 1502 (1984). [17]S. K. Cheung and N. W. Cheung, Appl. Phys. Lett. 49, 85 (1986).

[18] J. H. Werner, Appl. Phys. A: Solids Surf. 47, 291 (1988).

[19]T. C. Lee, S. Fung, C. D. Beiling, and H. L. Au, J. Appl. Phys. 72, 4739 (1992).

[20]D. Gromov and V. Pugachevich, Appl. Phys. A: Solids Surf. 59, 331 (1994).

[21]V. Aubry and F. Meyer, J. Appl. Phys. 76, 7973 (1994).

[22]V Mikhelashvili, G Eisenstein, V Garber, S Fainleib, G Bahir, D Ritter,J. Appl. Physics, 85, 6873 (1999).

[23]K. Maeda, H. Ikoma, K. Sato, T. Ishida, Appl. Phys. Lett., 62, 2560 (1993).

[24]T. Ishida, H. Ikoma, J. Appl. Phys., 74, 3977 (1993).

[25]V Mikhelashvili, G Eisenstein, R Uzdin, Solid-State Electronics 45, 143 (2001).

[26] E.H. Rhoderick, R.H. Williams, Metal–Semiconductor Contacts, Oxford University Press, USA, 1988.

[27]C.-Y. Wu, J. Appl. Phys., 51, 3786 (1980).

[28] C.-Y. Wu, J. Appl. Phys., 53, 5947 (1982).

[29] E.H. Nicolian and J. R. Brews, MOS Physics and Technology, (J. Wiley, New York (1982).

[30] C. Barret and A. Vapaille, Solid State Electron., 18, 25 (1975).

[31]V. Mikhelashvili, Y. Betzer I. Prudnikov, M. Orenstein, D. Ritter, G. Eisenstein, J Appl Phys., 84, 6747 (1998).

[32]Y. Liu, J. Yu, W. M. Tang, and P. T. Lai, Appl. Phys. Lett. 105, 223503 (2014).

[33] K. Murakami, M. Rommel, V. Yanev, T. Erlbacher, A. J. Bauer, and L. Frey, J. App. Phys., 110, 054104 (2014).

[34] P. Smertenko, L. Fenenko, L. Brehmer, S. Schrader, Advances in colloid and interface science, 116, 255 (2005).

[35] O. Ya. Olikh, J. of Appl. Phys., 118, 024502 (2015).

[36]C. Acha, J. Appl. Phys., 121, 134502 (2017).

[37]M. Lyakas, R. Zaharia, M. Eizenberg, J. Appl. Phys., 78, 5481 (1995).

[38] M. A. Lampert and P. Mark, Current Injection in Solids (Academic Press, New York, 1970).

[39]J.W. Schwede, I. Bargatin, D.C. Riley, B.E. Hardinm, S.J.Rosental, Y. Sun, F. Schmitt, P. Pianetta, R.T. Howe, Z. Shen and N.A. Melosh, Nat. Mater., 9, 762 (2010).

[40] M.-Y. Lu, M.-P. Lu, S.-J. You, C.-W. Chen and Y.-J. Wang, Scientific Reports, 5, 15123 (2015).

[41]A. K. Sharma, S. N. Singh, Nandan S. Bisht, H. C. Kandpal, and Z. H. Khan, Sol. Energy Mater. Sol. Cells 100, 48 (2012).

[42] S.I. Pekar, Zh Eksper i Teoret Fiziki, 10, 1210 (1940) [in Russian].

[43] S.I. Pekar, Zh Eksper i Teoret Fiziki, 11, 708 (1941) [in Russian].

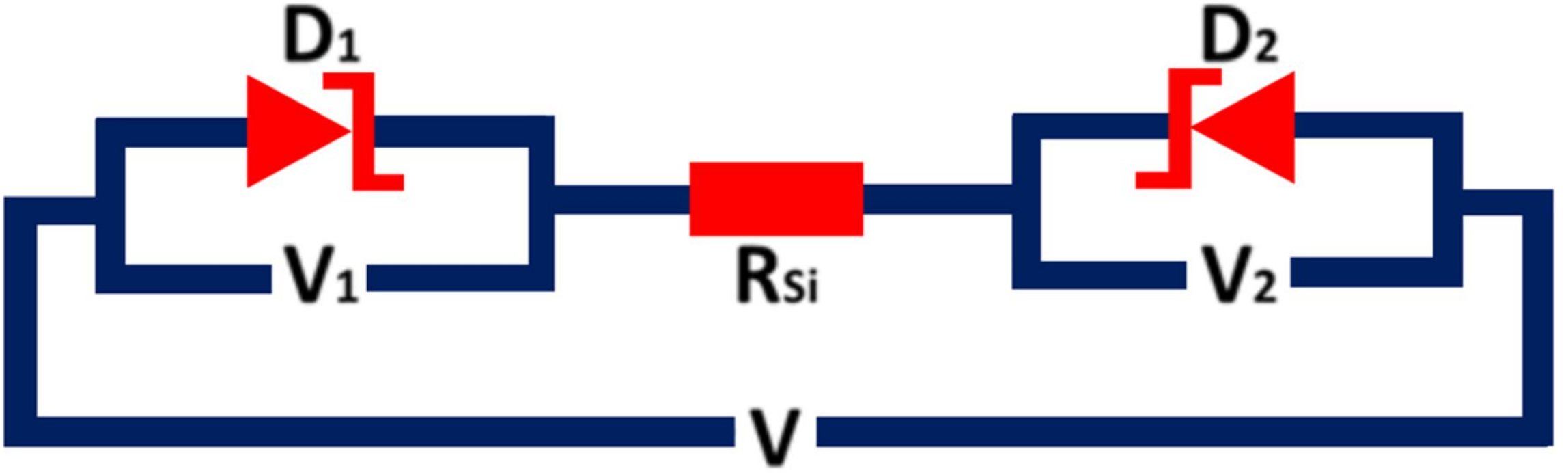
D1
D2
V1
RSi
V2
V

(a)

3x10^-11
2x10^-11
1x10^-11
0.0
-1x10^-11
-2x10^-11
-3x10^-11

Current (A)

-5 -4 -3 -2 -1 0 1 2 3 4 5

Applied voltage (V)

1
2
3
4

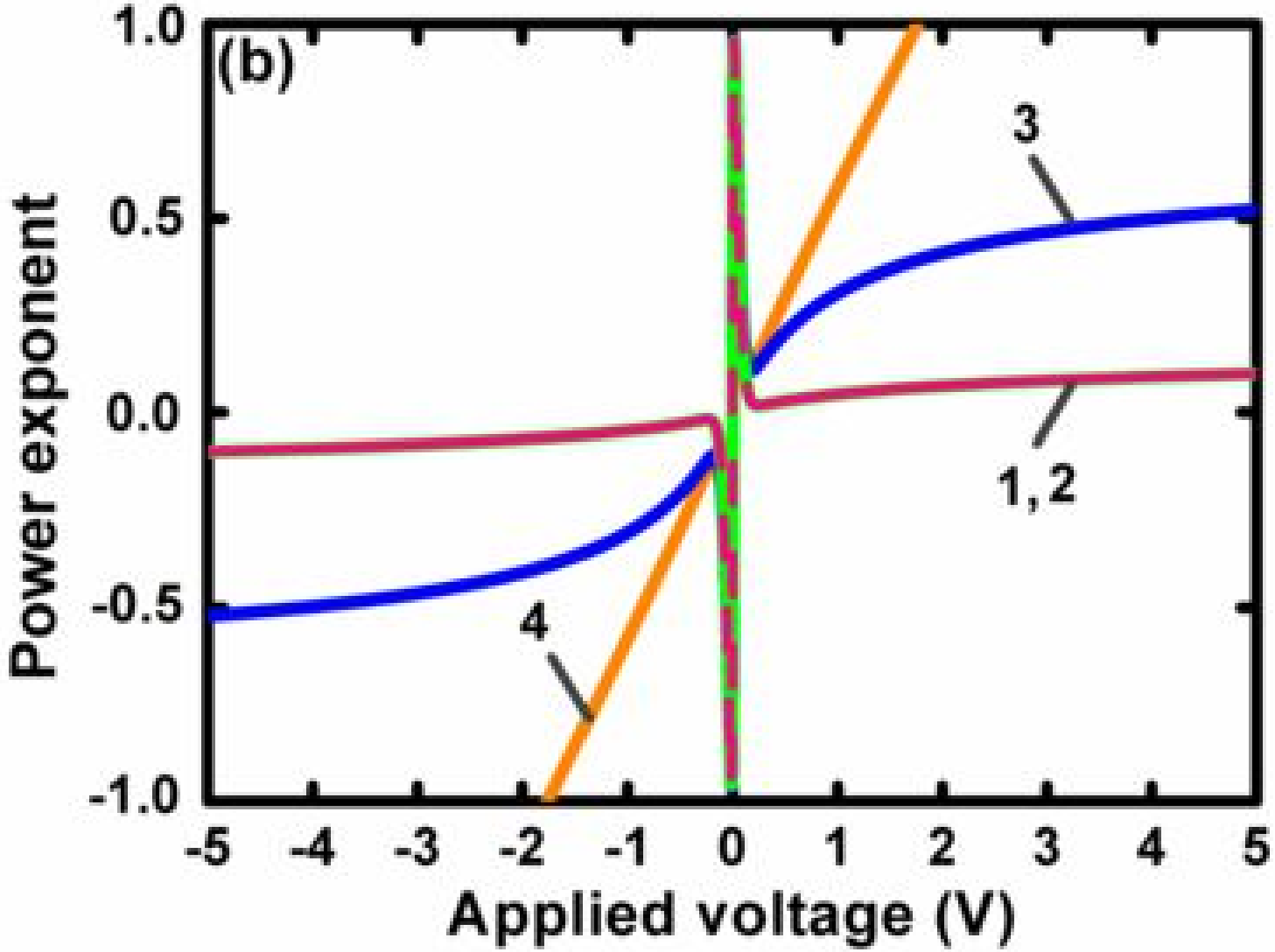
(b)
Power exponent
Applied voltage (V)
1.0
0.5
0.0
-0.5
-1.0
-5
-4
-3
-2
-1
0
1
2
3
4
5
3
1, 2
4

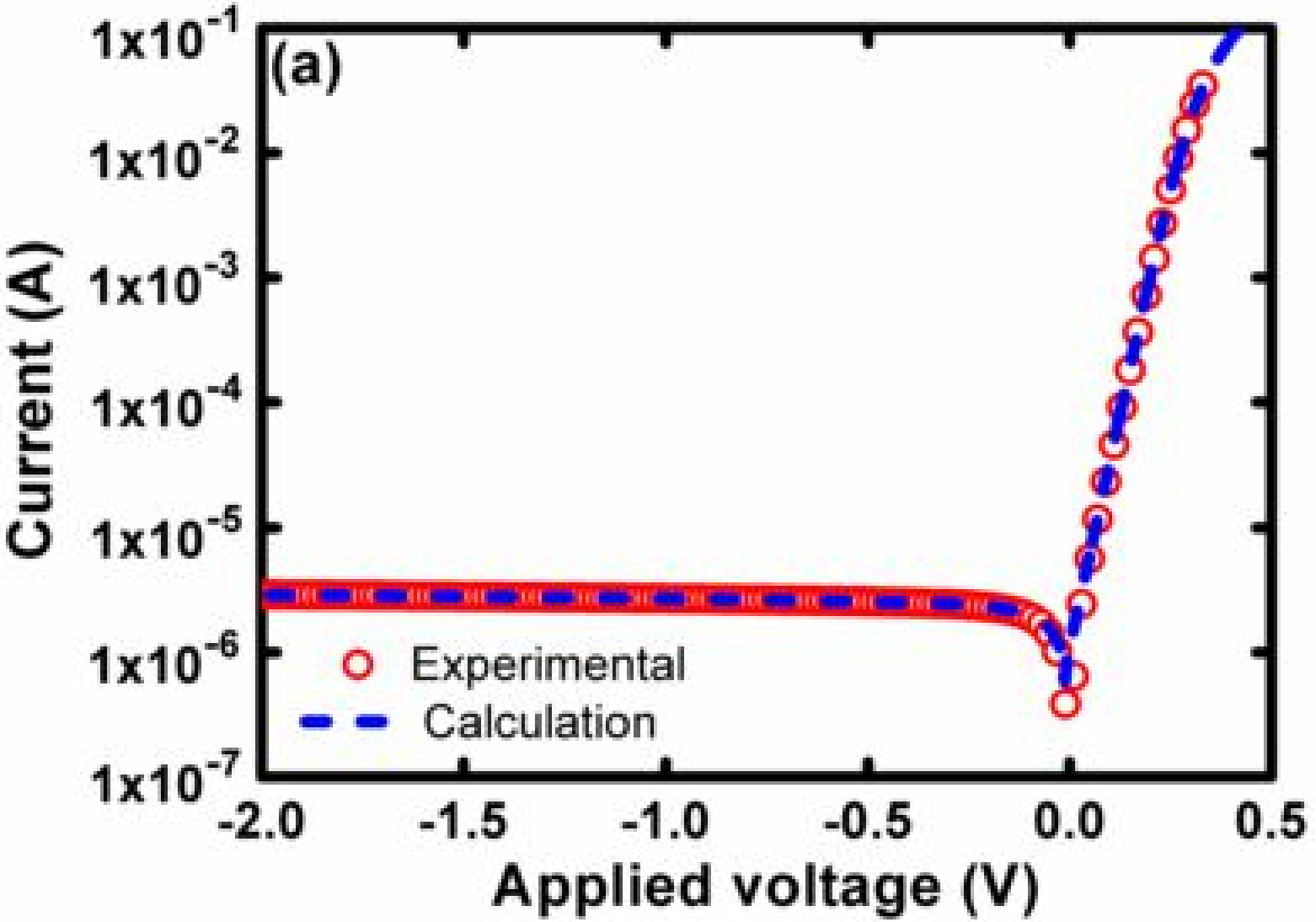
(a)
Current (A)
1x10^-1
1x10^-2
1x10^-3
1x10^-4
1x10^-5
1x10^-6
1x10^-7
Experimental
Calculation
-2.0
-1.5
-1.0
-0.5
0.0
0.5
Applied voltage (V)

(b)

Power exponent

Applied voltage (V)

Experimental

Calculation

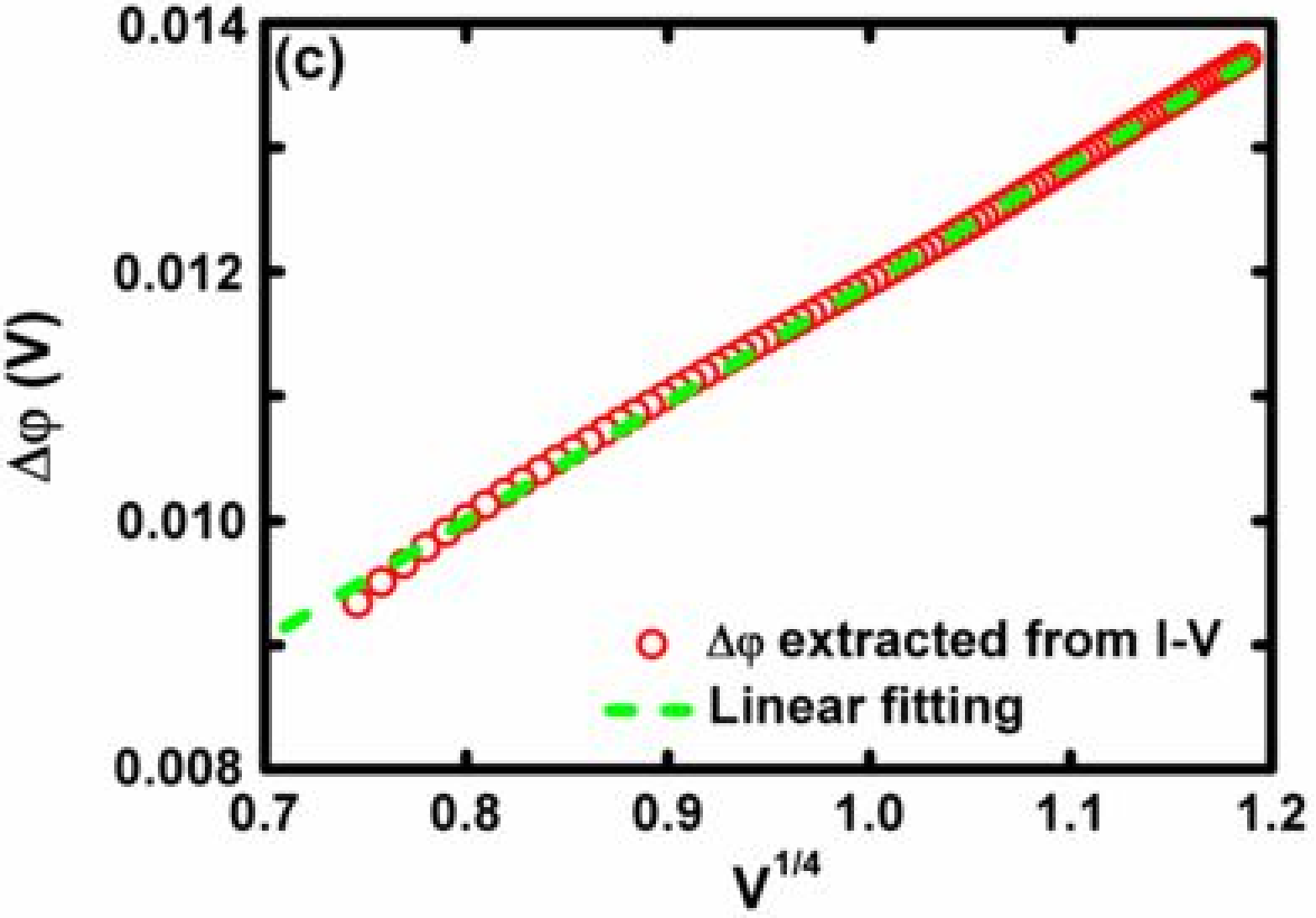
(c)
0.014
0.012
0.010
0.008
Δφ (V)
0.7
0.8
0.9
1.0
1.1
1.2
V^1/4
Δφ extracted from I-V
Linear fitting

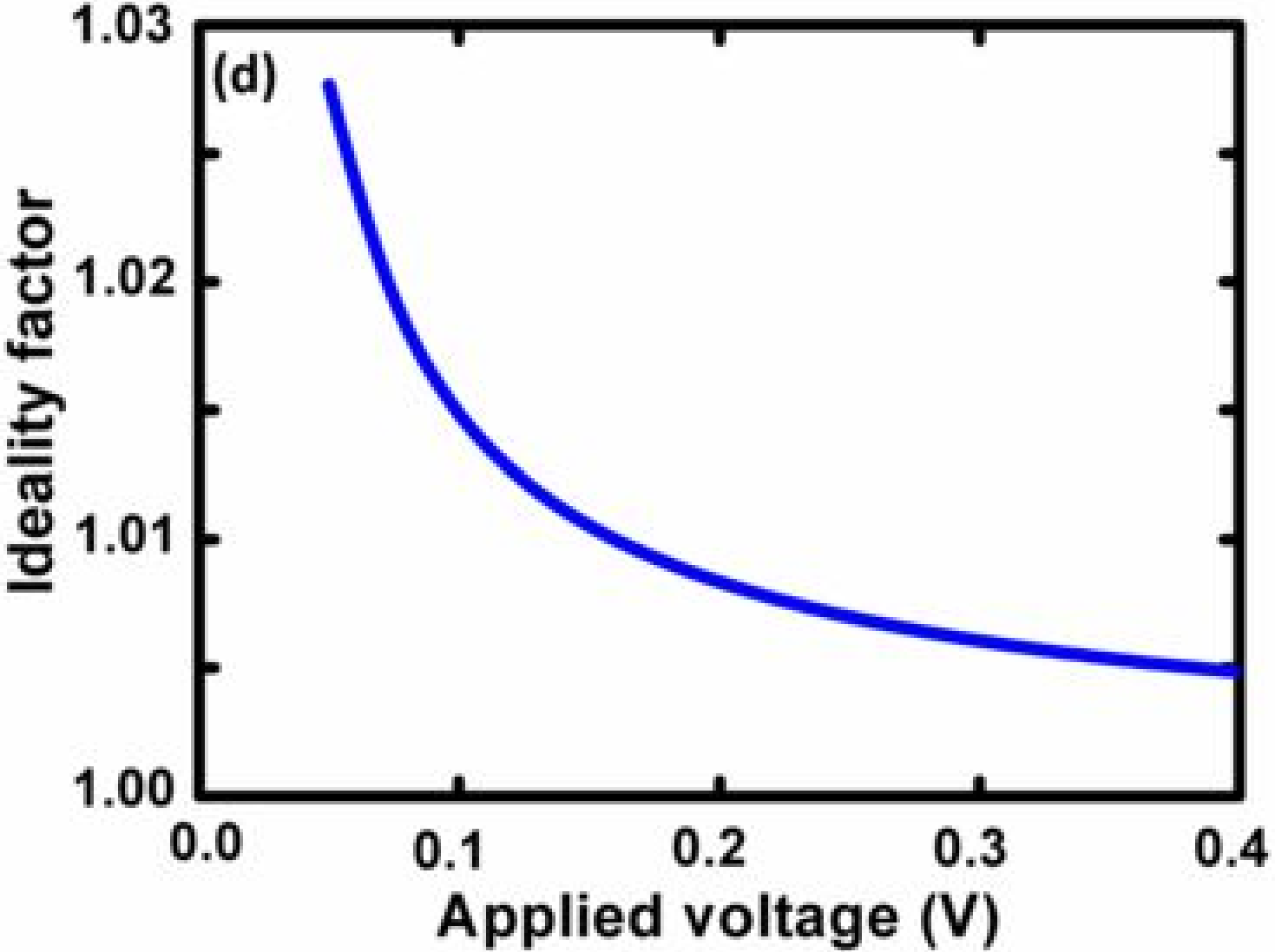
(d)
Ideality factor
1.03
1.02
1.01
1.00
0.0
0.1
0.2
0.3
0.4
Applied voltage (V)

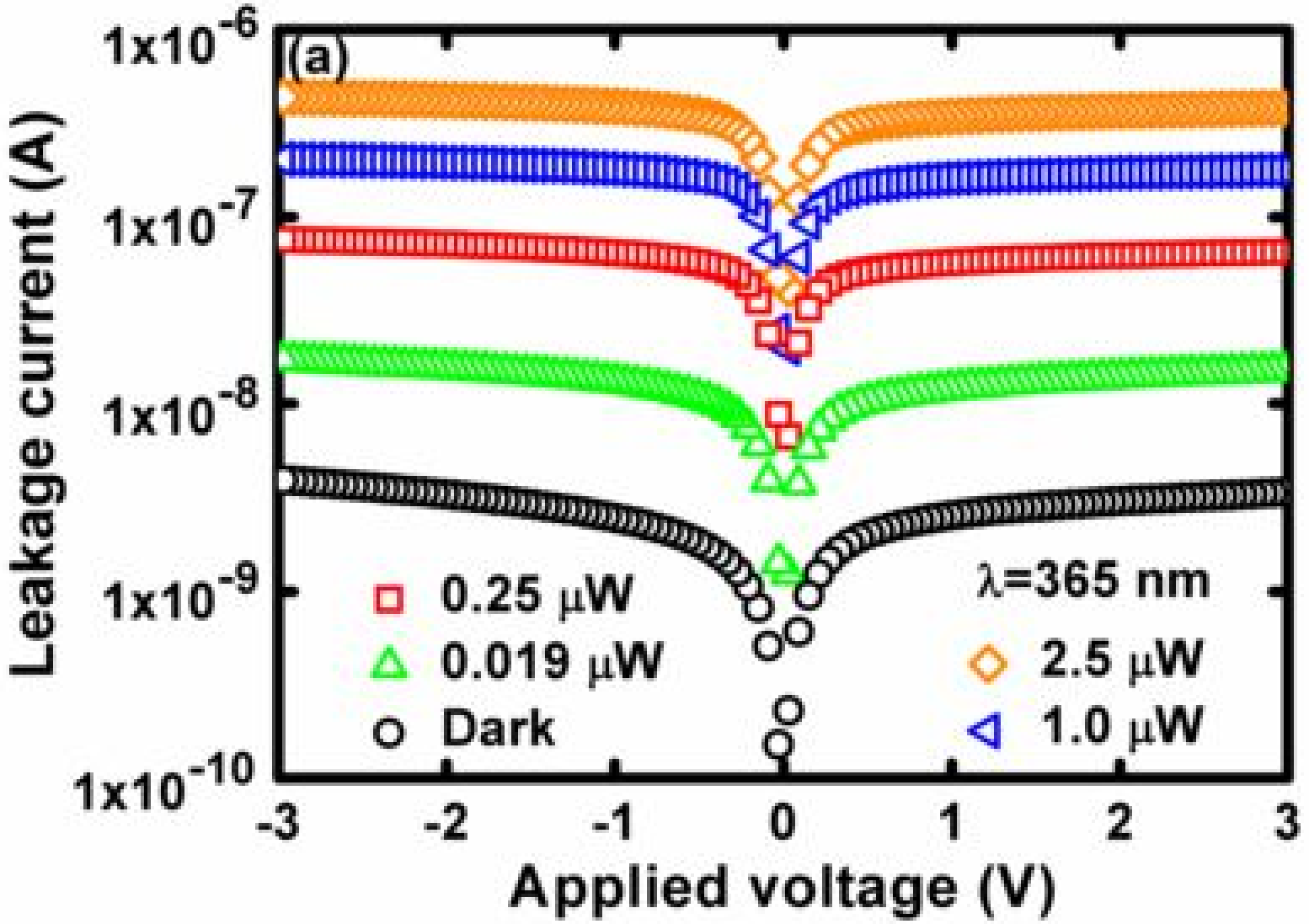
(a)
Leakage current (A)
1x10-6
1x10-7
1x10-8
1x10-9
1x10-10
-3
-2
-1
0
1
2
3
Applied voltage (V)
λ=365 nm
0.25 μW
0.019 μW
Dark
2.5 μW
1.0 μW

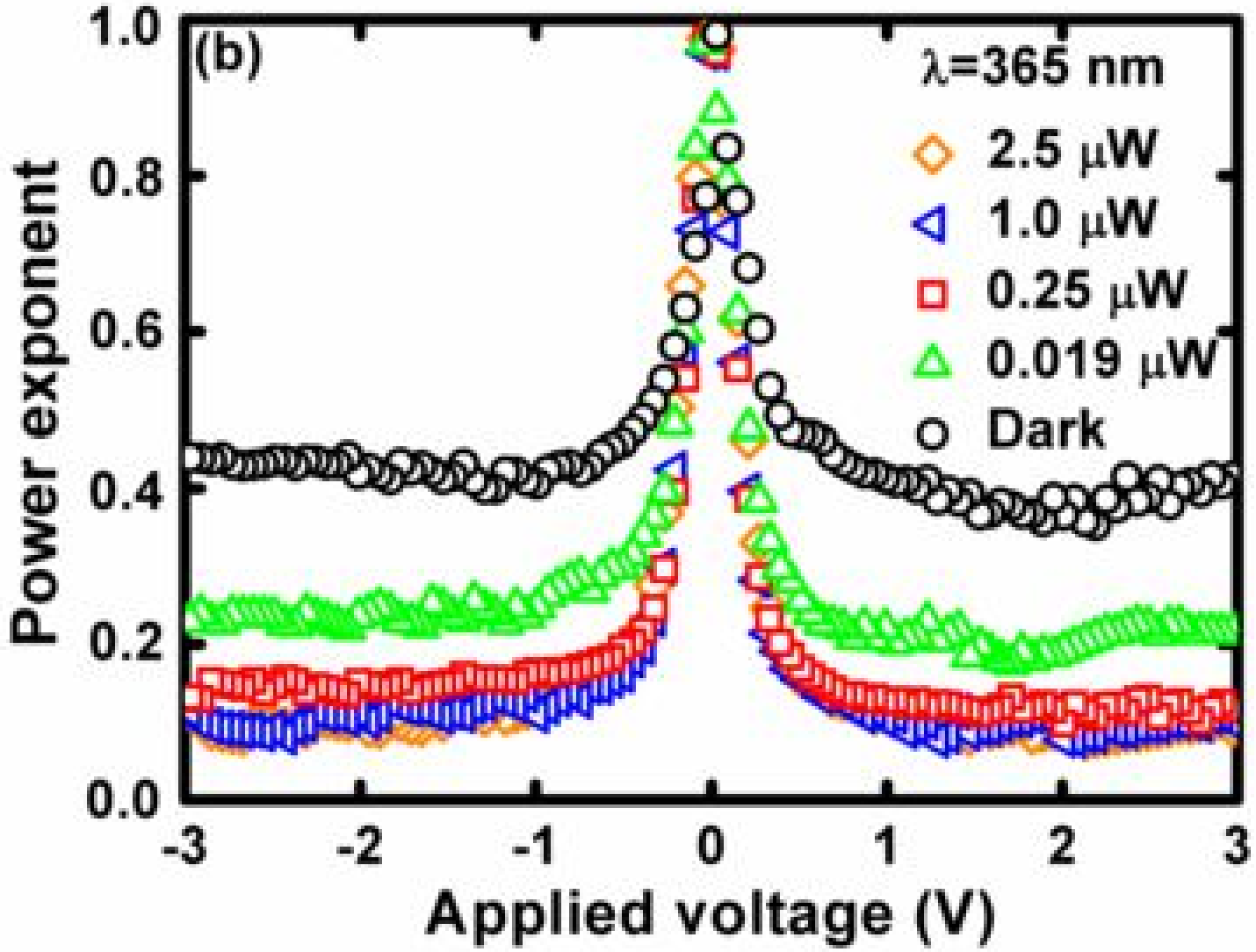
(b)
λ=365 nm
2.5 μW
1.0 μW
0.25 μW
0.019 μW
Dark
Power exponent
Applied voltage (V)
1.0
0.8
0.6
0.4
0.2
0.0
-3
-2
-1
0
1
2
3

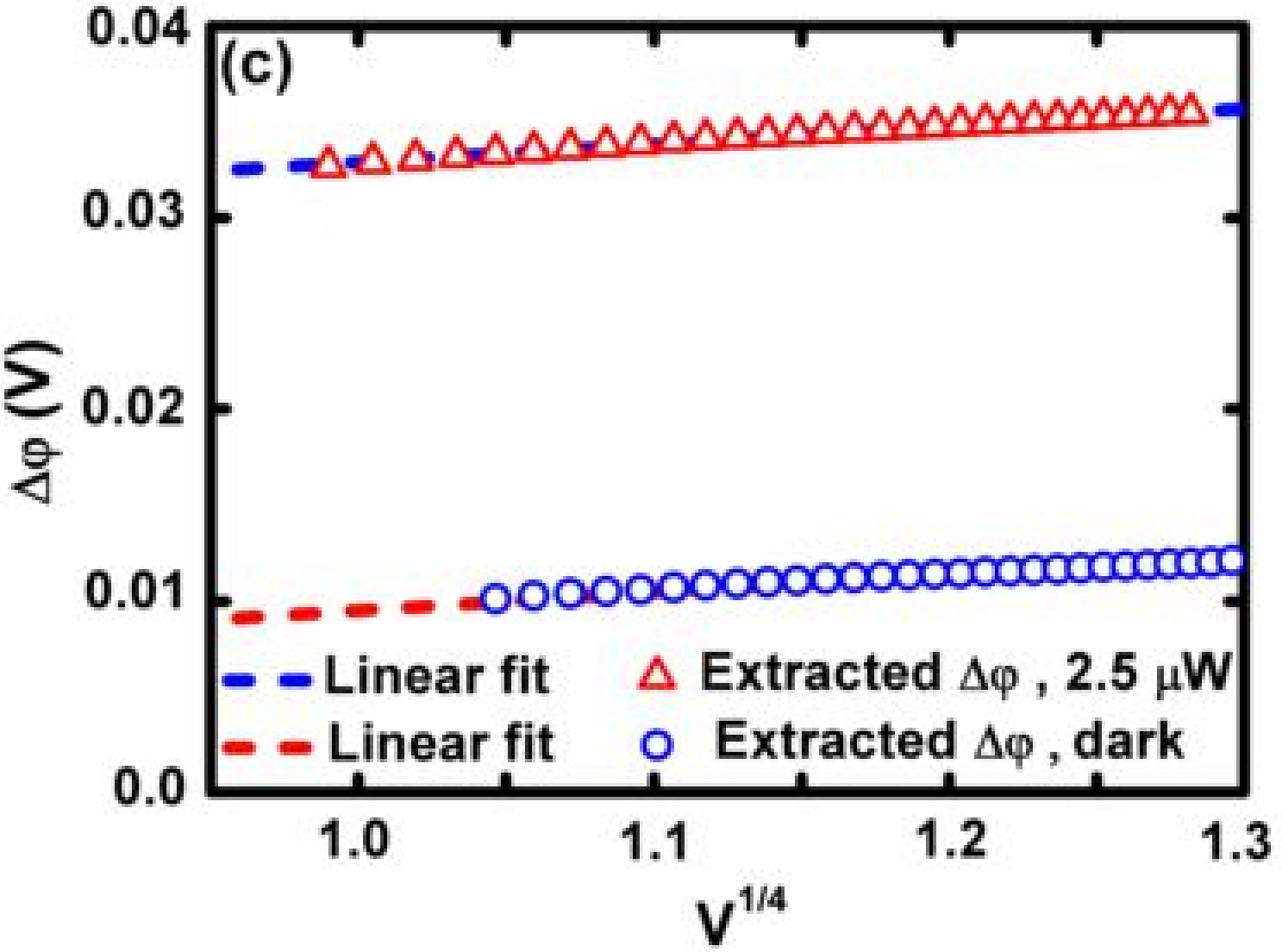
(c)
0.04
0.03
0.02
0.01
0.0
Δφ (V)
1.0
1.1
1.2
1.3
V^1/4
Linear fit
Linear fit
Extracted Δφ , 2.5 μW
Extracted Δφ , dark

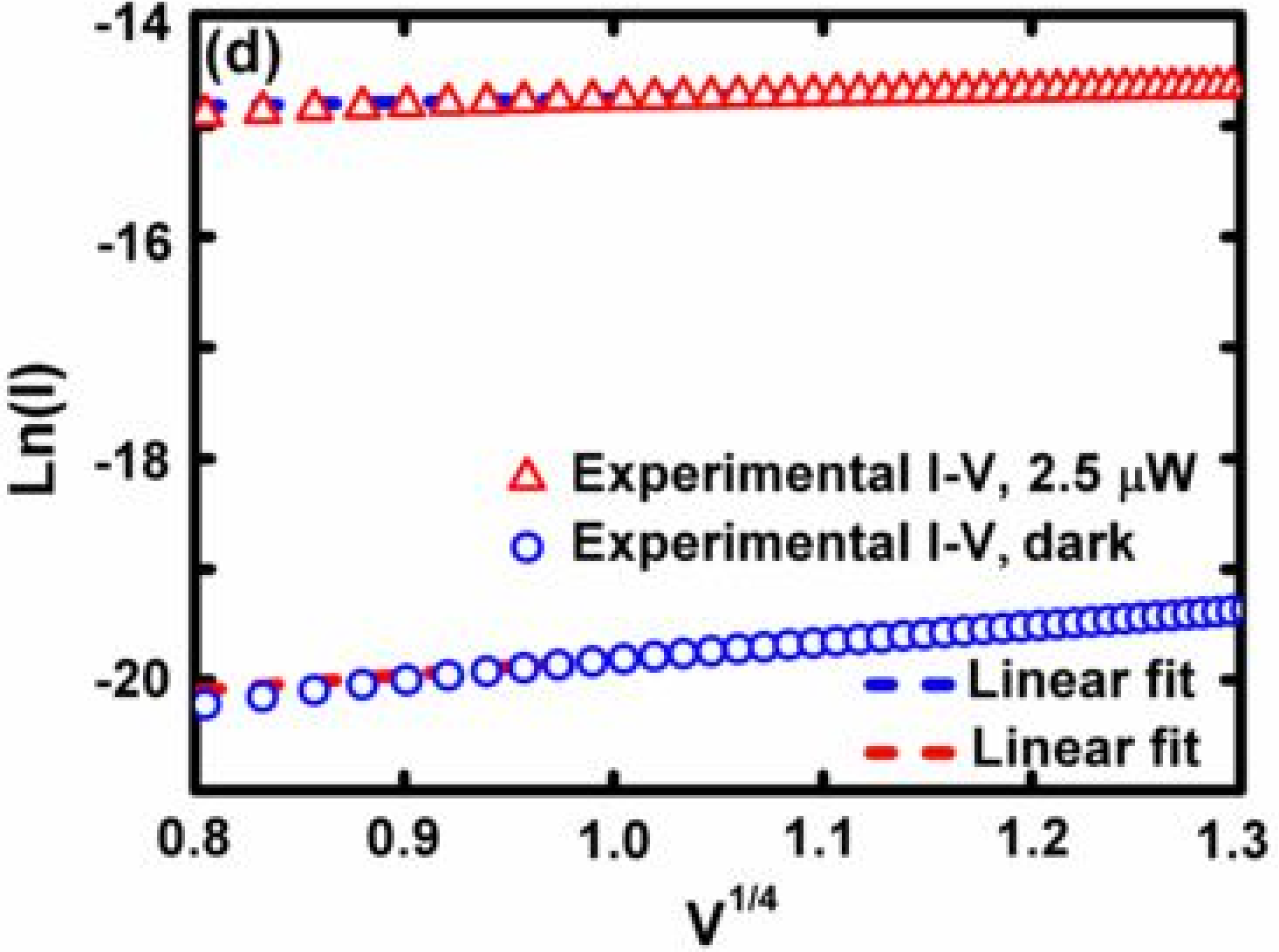
(d)
-14
-16
-18
-20
Ln(I)
0.8
0.9
1.0
1.1
1.2
1.3
V^1/4
Experimental I-V, 2.5 μW
Experimental I-V, dark
Linear fit
Linear fit

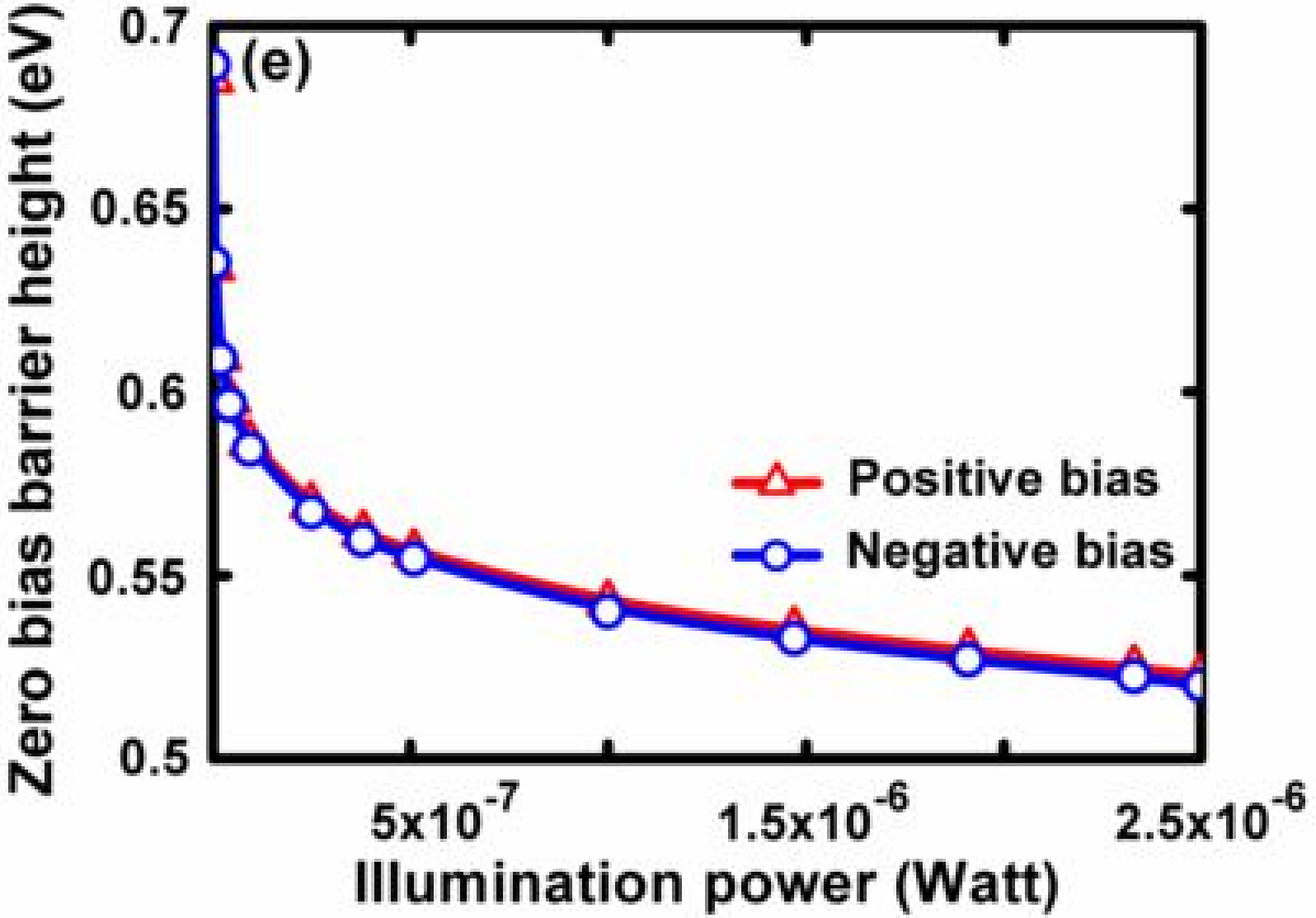
(e)
0.7
0.65
0.6
0.55
0.5
Zero bias barrier height (eV)
Positive bias
Negative bias
5x10^-7
1.5x10^-6
2.5x10^-6
Illumination power (Watt)

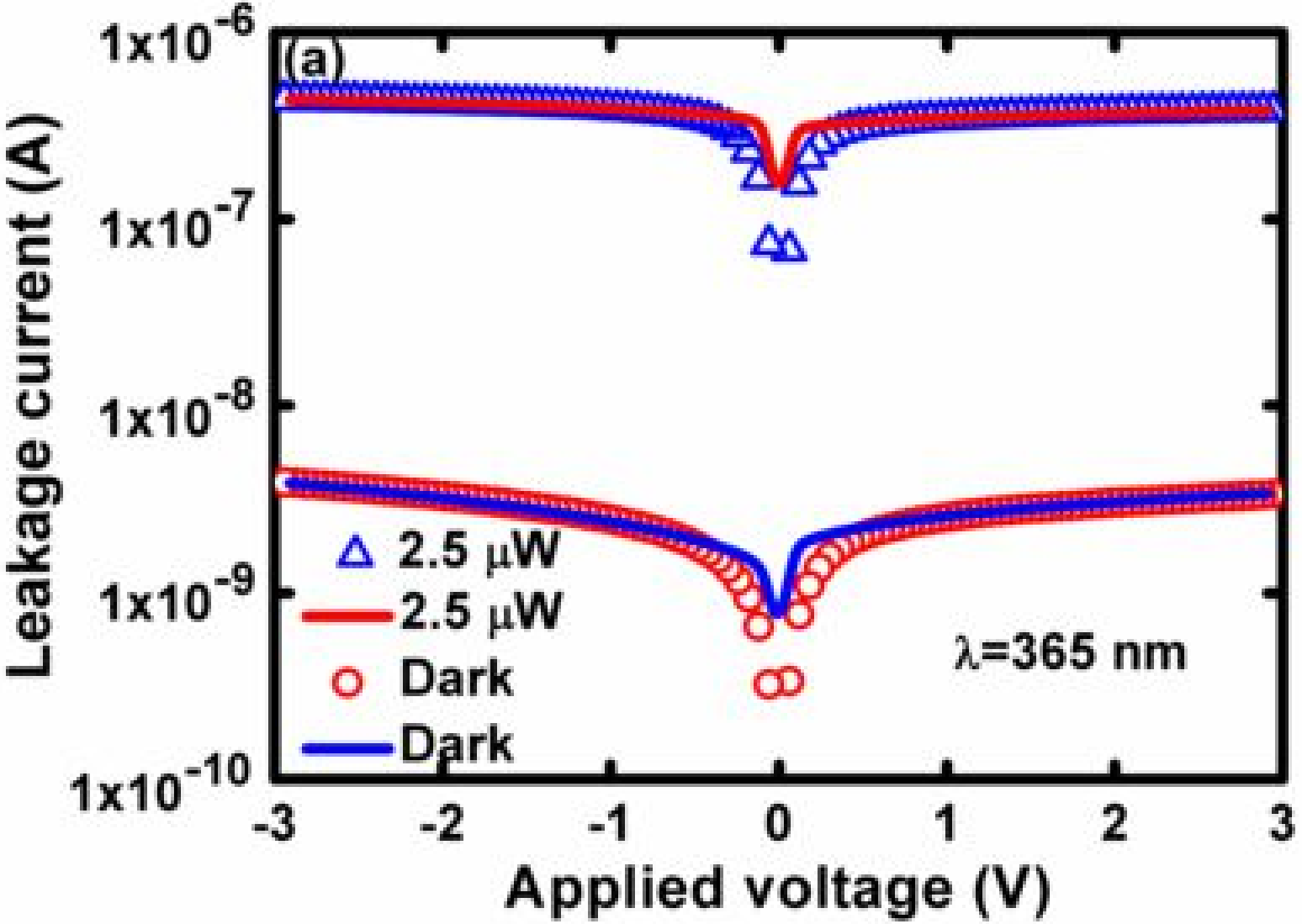
(a)
1x10^-6
1x10^-7
1x10^-8
1x10^-9
1x10^-10
Leakage current (A)
-3
-2
-1
0
1
2
3
Applied voltage (V)
2.5 μW
2.5 μW
Dark
Dark
λ=365 nm

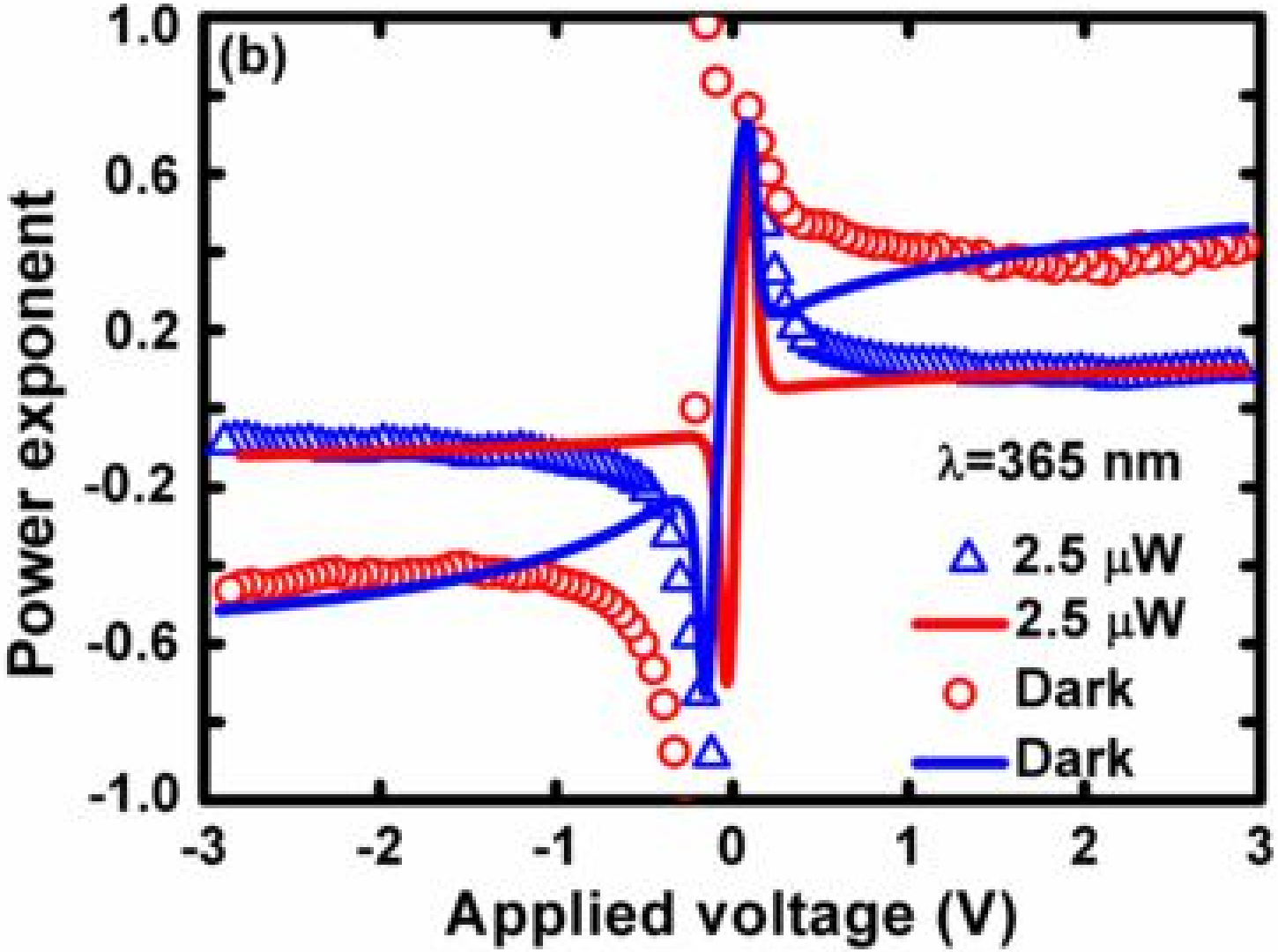
(b)
Power exponent
Applied voltage (V)
1.0
0.6
0.2
-0.2
-0.6
-1.0
-3
-2
-1
0
1
2
3
λ=365 nm
2.5 μW
2.5 μW
Dark
Dark

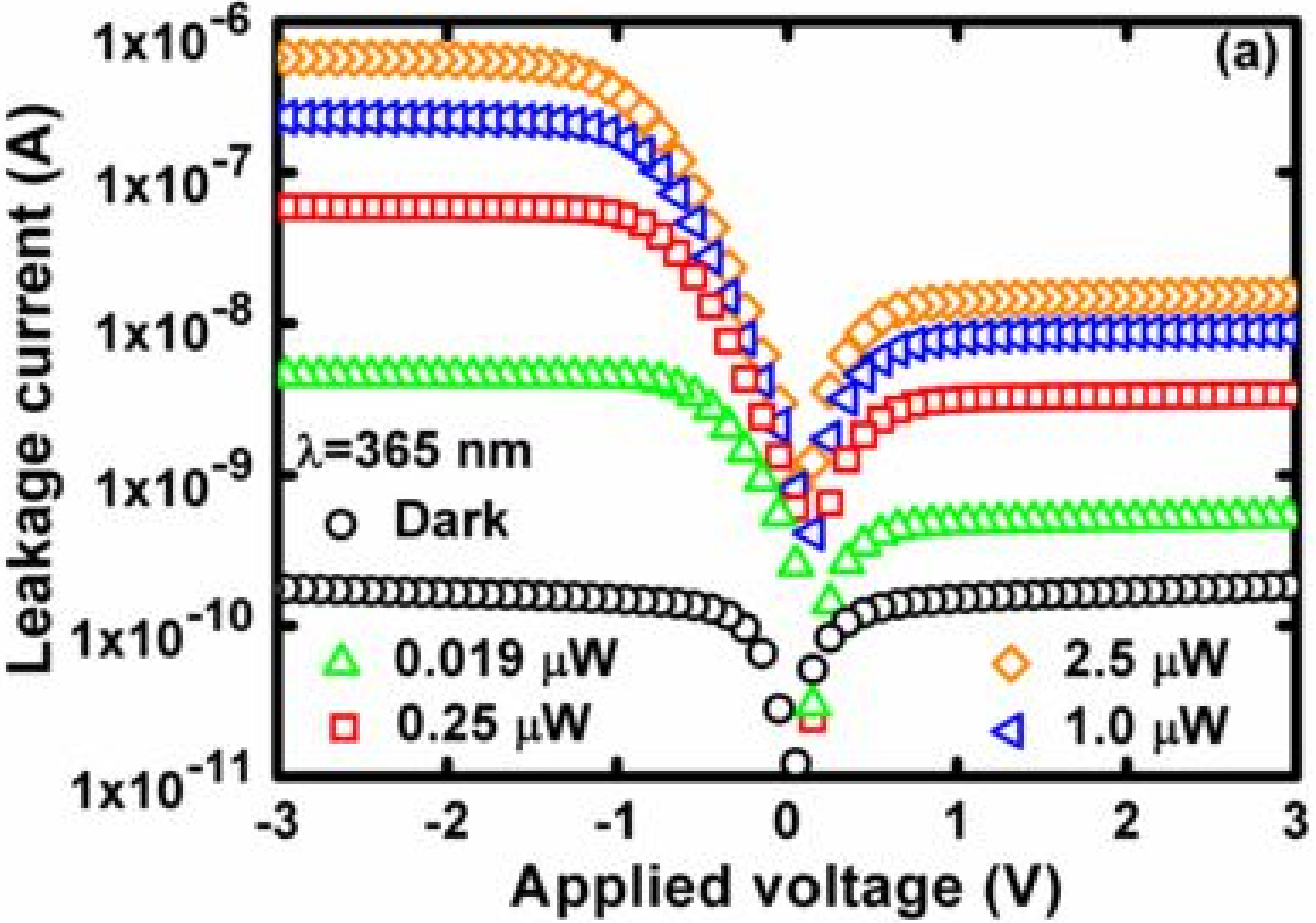
(a)
Leakage current (A)
1x10-6
1x10-7
1x10-8
1x10-9
1x10-10
1x10-11
λ=365 nm
Dark
0.019 μW
0.25 μW
2.5 μW
1.0 μW
-3
-2
-1
0
1
2
3
Applied voltage (V)

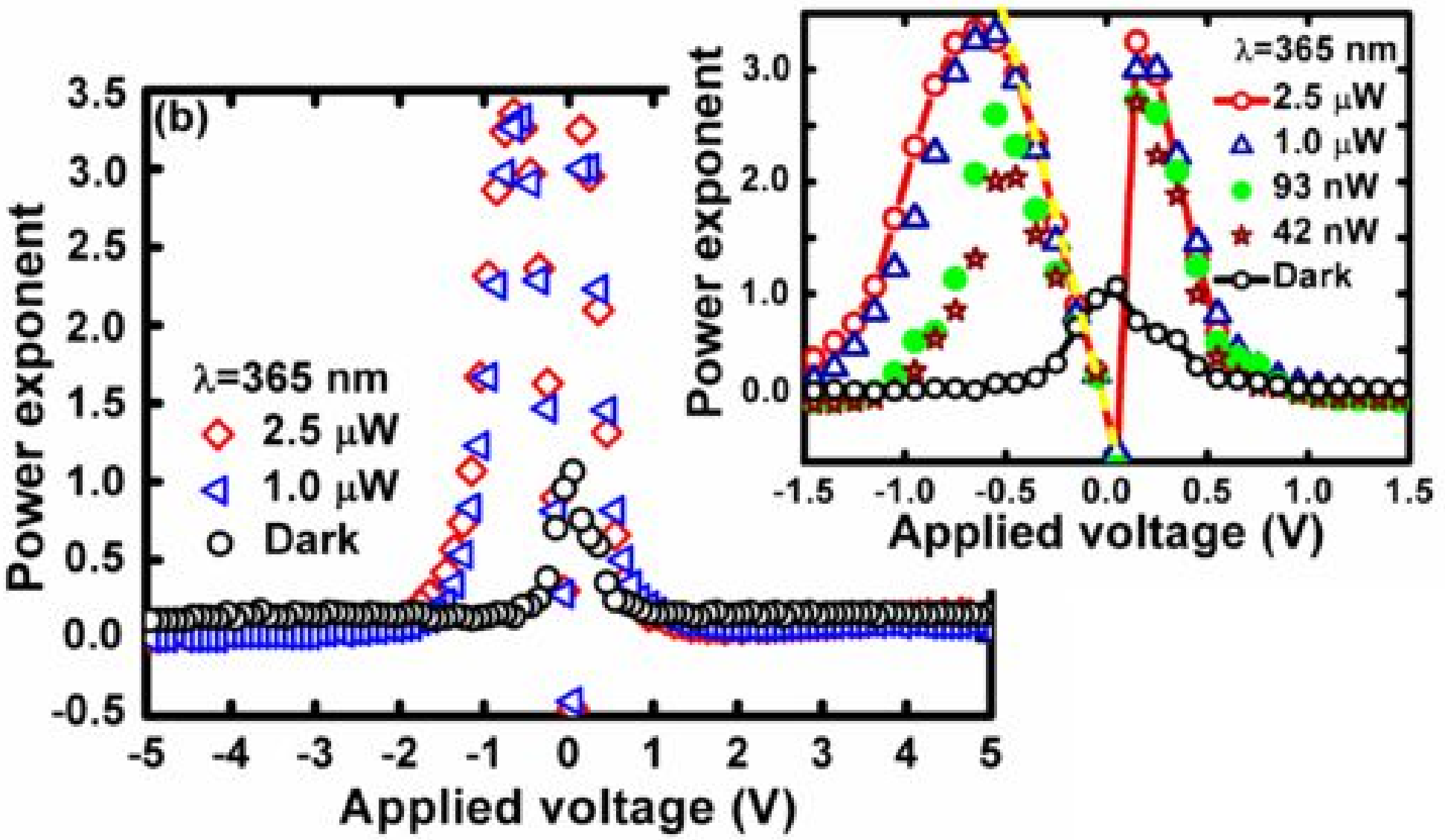
(b)
Power exponent
Applied voltage (V)
λ=365 nm
2.5 μW
1.0 μW
Dark
93 nW
42 nW

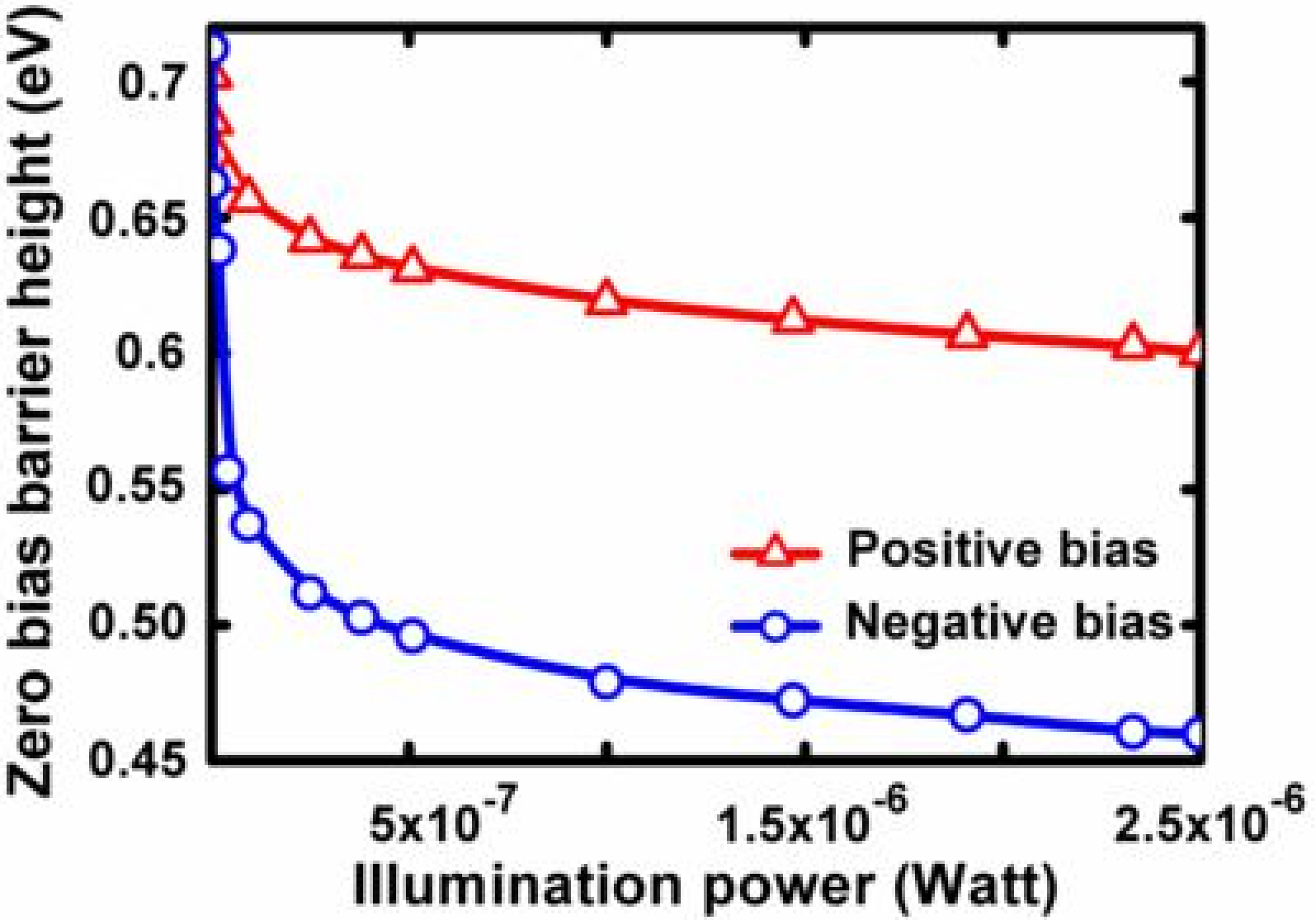
Zero bias barrier height (eV)
0.7
0.65
0.6
0.55
0.50
0.45
Positive bias
Negative bias
5x10-7
1.5x10-6
2.5x10-6
Illumination power (Watt)